HHS Public Access

Author manuscript

Dev Biol. Author manuscript; available in PMC 2024 December 17.

Published in final edited form as:

Dev Biol. 2022 November ; 491: 31–42. doi:10.1016/j.ydbio.2022.08.003.

Deciphering the role of retinoic acid in hepatic patterning and induction in the mouse

Taylor M. Guertin[1], **Amrita Palaria**[1], **Jesse Mager**[1], **Lisa L. Sandell**[2], **Paul A. Trainor**[3,4], **Kimberly D. Tremblay**[1,*]

[1]Department of Veterinary and Animal Sciences, University of Massachusetts, Amherst, MA, USA

[2]Department of Oral Immunology and Infectious Diseases, School of Dentistry, University of Louisville, Louisville, KY, USA

[3]Stowers Institute for Medical Research, Kansas City, MO, USA

[4]Department of Anatomy and Cell Biology, School of Medicine, University of Kansas, Kansas City, KS, USA

Abstract

Retinoic acid (RA), a metabolite of vitamin A, is a small molecule and morphogen that is required for embryonic development. While normal RA signals are required for hepatic development in a variety of vertebrates, a role for RA during mammalian hepatic specification has yet to be defined. To examine the requirement for RA in murine liver induction we performed whole embryo culture with the small molecule RA inhibitor, BMS493, to attenuate RA signaling immediately prior to hepatic induction and through liver bud formation. BMS493-treated embryos demonstrated a significant loss of hepatic specification that was confined to the prospective dorsal anterior liver bud. Examination of RA-attenuated embryos demonstrates that while the liver bud displays normal expression of foregut endoderm markers and the hepato-pancreatobiliary domain marker, PROX1, the dorsal/anterior liver bud excludes the critical hepatic marker, HNF4α, indicating that RA signals are required for dorsal/anterior hepatic induction. These results were confirmed and extended by careful examination of *Rdh10*$^{trex/trex}$ embryos, which carry a genetic perturbation in RA synthesis. At E9.5 *Rdh10*$^{trex/trex}$ embryos display a similar yet more significant loss of the anterior/dorsal liver bud. Notably the anterior/dorsal liver bud loss correlates with the known dorsal-ventral gradient of the RA synthesis enzyme, *Aldh1a2*. In addition to altered hepatic specification, the mesoderm surrounding the liver bud is disorganized in RA abrogated embryos. Analysis of E10.5 *Rdh10*$^{trex/trex}$ embryos reveals small livers that appear to lack the dorsal/caudal lobes. Finally, addition of exogenous RA prior to hepatic induction results in a liver bud that has failed to thicken and is largely unspecified. Taken together our *ex vivo* and *in vivo* evidence demonstrate that the generation of normal RA gradients is required for hepatic patterning, specification, and growth.

*Author for correspondence: Department of Veterinary and Animal Sciences, University of Massachusetts, Amherst, MA, USA, kdtrembl@umass.edu.

Supplemental Information

Immunofluorescence

Immunofluorescence was performed as described in the main text but with the following primary antibody and working dilution; mouse anti-Foxa1 (Seven Hills Bioreagents, WMAB-2F83, 1:500).

Introduction

The liver is the largest internal organ in the human body and is essential for performing critical metabolic, exocrine and endocrine functions, which include bile production and secretion, metabolism of fats, proteins and carbohydrates, glycogen storage and regulation of glucose levels, blood detoxification and homeostasis and synthesis of plasma proteins. Hepatocytes, the most prominent cell type in the liver, comprise up to 70% of the adult organ and are derived from embryonic endoderm.

The endoderm emerges during gastrulation as an epithelial sheet on the ventral surface of the developing mouse embryo. Liver induction initiates at ~E8.25 and by E8.75 the hepatic endoderm has thickened and begun to evaginate from the remainder of the gut epithelium to form the liver bud. By E9.5 the cells of the liver bud, termed hepatoblasts, can be distinguished by the expression of liver specific genes including hepatocyte nuclear factor 4-alpha (*Hnf4α*) and alpha-fetoprotein (*Afp*).

Hepatic induction requires growth factors secreted from adjacent mesoderm-derived tissues. Two of these factors include bone morphogenic protein (BMP), believed to be produced by the septum transversum mesenchyme (STM), and fibroblast growth factor (FGF) presumed to emanate from the cardiac mesoderm. While it has been assumed that both factors are uniformly and simultaneously required for the emergence of hepatic progenitors from the naïve endoderm, recent experiments demonstrate that spatially distinct populations of pre-hepatic endoderm have differential requirements for each pathway (Palaria et al., 2018; Wang et al., 2015). For example, abrogation of the FGF pathway results in the failure to specify the anterior-most portion of the nascent liver bud, while abrogation of the BMP pathway leads to a significant loss of the posterior-most portion of the liver bud. Intriguingly, simultaneous abrogation of both the BMP and FGF signaling pathways result in a dramatic, but not complete, reduction of hepatoblasts, suggesting that other signaling pathways may be involved in hepatic induction (Palaria et al., 2018).

One candidate for this signal that has not been fully examined in mammals includes, the Retinoic acid (RA) signaling pathway. RA has been shown to play a role in liver development in other vertebrates. For example, RA inhibition leads to a loss or severe reduction of liver markers in zebrafish and medaka (Negishi et al., 2010; Stafford and Prince, 2002) and exogenous RA treatment leads to liver ablation or a reduction of liver markers in *Xenopus* and chick, respectively (Bayha et al., 2009; Chen et al., 2004).

RA is a morphogen that is essential for normal embryonic development and has been shown to play a key role in the development of other mammalian foregut derivatives. RA is a small molecule metabolite of Vitamin A (retinol) and thus, sources of this crucial signal within the embryo are dependent on maternal circulation. Once passed through the maternal-fetal barrier, retinol must undergo two oxidation steps to become the biologically active signaling molecule RA. While many enzymes can catalyze these reactions, retinol dehydrogenase 10 (RDH10) and retinaldehyde dehydrogenase 2 (RALDH2 also termed ALDH1A2) are the main enzymes that catalyze these sequential reactions during embryogenesis (Farjo et

al., 2011; Kumar et al., 2012; Mic et al., 2002; Niederreither et al., 1997; Sandell et al., 2007). RA can translocate into the nucleus and bind to the RA receptors (RARs) which are present in a heterodimeric complex with retinoid X receptors (RXRs) bound to retinoic acid response elements (RAREs) in target genes. Given RA's role as a morphogen, the balance between RA synthesis and degradation within the embryo is tightly controlled to produce concentration gradients that are read by cells to induce specific patterns of gene expression that regulate proper embryonic development.

RA signaling is required for specification of the murine lungs and dorsal pancreas, two other organs that like the liver, derive from the foregut (Desai et al., 2004; Martin et al., 2005; Molotkov et al., 2005). Mid-gestation (E10.5-E13) embryos with impaired RA signaling exhibit absent or severely hypoplastic lungs, liver, pancreas, stomach, and duodenum (Sandell et al., 2007; Wang et al., 2006). Similarly, a severely reduced liver is observed in E12.5 *Rxra* mutant embryos (Sucov et al., 1994). Thus despite that these later defects are observed upon abrogation of RA signaling during development, a role for RA signaling during hepatic specification in mice has not yet been described.

Herein we examined the role RA plays during hepatic induction in the mouse. Culture of pre-hepatic (E8.25) embryos with the RA inhibitor BMS493 allows for strict temporal control of RA signal attenuation, specifically during the developmental window that encompasses hepatic induction and the onset of liver bud formation. RA inhibition during culture produces a marked loss of the anterior portion of the liver bud, highlighting the importance of RA signals for proper hepatic specification. Analysis of gut markers after RA inhibition demonstrates that the dorsal portion of the anterior liver bud is not specified. This defect was further confirmed via analysis of $Rdh10^{trex/trex}$ mutant embryos that almost completely lack RA signaling activity. Intriguingly, an excess of RA produces an even more severe impairment of the entire liver bud. Together these results establish that appropriate gradients of RA are essential for the proper specification of the liver bud during mammalian development.

Results

Expression of RA receptors in the liver progenitors and early liver bud

If RA signals play a direct role in early liver development, we expect that an RA gradient would be present in proximity to the liver progenitors and early liver bud and that these hepatic endoderm derived cells are capable of responding to RA. Fate mapping experiments have shown that the nascent liver bud is comprised of two pre-hepatic populations of liver progenitors, the ventral midline of the endoderm lip (VMEL) and the lateral progenitors that merge together by E8.5 (Tremblay and Zaret, 2005). We focused our expression analysis on both liver progenitor populations at E8.5, when specified hepatoblasts can be first detected, and in the E9.5 liver bud (Fig. 1). RA binds specifically to a RAR which heterodimerizes with an RXR in the nucleus and there are three isoforms of each receptor. *Rarα* expression is detected in both the VMEL and lateral progenitors at E8.5, and at E9.5 is diffusely expressed in the liver bud and adjacent mesoderm (Fig. 1A). At E8.5 *Rarβ* is expressed in the dorsal endoderm and is more highly expressed in the hepatic progenitors than in the surrounding mesoderm. By 9.5 *Rarβ* is expressed in the gut tube and surrounding

mesoderm but is absent in the hepatic endoderm and surrounding mesoderm (Fig. 1B). *Rarγ* was not examined because its expression is restricted to the first branchial arch and tail bud (Abu-Abed et al., 2003). *Rxrα,* the only RA receptor that is critical for embryonic development, is expressed in the VMEL and lateral progenitors (Sucov et al., 1994). At E9.5 *Rxrα* is diffusely expressed throughout the embryo, except the heart, and is expressed in both the liver bud and adjacent mesoderm (Fig. 1C). Together, the expression of at least one RAR and RXR in the liver progenitors at the time of hepatic specification and in the early liver bud indicates that both can respond to and thus be directly affected by RA signals.

Examination of the expression of essential RA synthesis enzymes reveals an endogenous dorsal to ventral gradient of RA. *Rdh10*, responsible for the oxidation of retinol to retinaldehyde, has a very specific pattern of expression that is high in both liver progenitor populations but is more diffusely expressed around the liver bud at E9.5 (Fig. 1D). Expression of *Aldh1a2*, which oxidizes retinaldehyde to retinoic acid, reveals a dorsal to ventral gradient of RA production in the mesoderm at the level of the developing liver bud [Fig. 1E; (Molotkov et al., 2005)]. Notably, *RARE-lacZ* expression, a transgenic reporter that allows for the presence of active RA signaling to be visualized by staining for β-galactosidase (Rossant et al., 1991), has shown that RA diffuses beyond the synthesis sites and that RA signaling is active throughout the dorsal endoderm (Molotkov et al., 2005). To identify the tissues that are responding to RA signal we X-gal stained *RARE-lacZ* embryos. At E8.5 *lacZ* expression is detected in the mesoderm adjacent to the hepatic progenitors but not in the hepatic endoderm (Fig. 1F), suggesting that if RA plays a role at the onset of hepatic induction it is likely indirect. However, by E9.5 *RARE-lacZ* activity is found in the dorsal portion of the liver bud and in the mesoderm adjacent to the dorsal liver bud (Fig. 1F), demonstrating that RA signals could play both a direct and indirect role in supporting early liver bud morphogenesis. Taken together the expression patterns documented above support the hypothesis that RA signals are poised to play a role in early mammalian hepatogenesis.

RA signaling inhibition leads to a loss of hepatic specification within the dorsal/anterior liver bud

To begin to understand the requirements for RA signaling during hepatic specification, we cultured murine embryos immediately prior to the onset of hepatic induction (E8.25; 4–6S) through the liver budding stage (E9.5; 24–28S) with the pan-RAR inverse agonist, BMS493 (Chazaud et al., 1999). This small molecule was used at the highest concentration that produced grossly normal embryos (20 μM; Fig. 2B). The effectiveness of BMS493 was confirmed by the absence of the third pharyngeal pouch and dorsal pancreas in BMS493 treated but not in control (DMSO only) cultured embryos [Fig. 2A, B and data not shown (Martin et al., 2005; Molotkov et al., 2005; Wendling et al., 2000)]. To probe potential liver defects, treated and control embryos were sectioned and immunofluorescence performed with several critical endoderm and hepatic specific markers (Fig. 2C, D). Examination of the pan-endodermal marker FOXA1 and the hepato-pancreatobiliary domain marker PROX1 reveals that FOXA1 and PROX1-positive cells uniformly populate the thickened hepatic domain of both control and BMS493 treated embryos (Fig. 2C, D; S Fig. 1), suggesting that the presumptive hepatic domain is appropriately patterned in the absence of RA signaling. HNF4α, a transcription factor that is essential for hepatic specification, is

noticeably downregulated in the anterior liver bud of BMS493 treated embryos (n = 22/25) when compared to controls (n = 2/26) (Fig. 2C, D). Upon closer examination of the anterior liver bud of treated embryos, HNF4α expressing cells are confined to the ventral-most half of the liver bud while HNF4α is absent in the PROX1-positive dorsal-most portion (Fig. 2D, white dashed lines). A similar dorsal loss is observed when examining the nonessential hepatoblast marker, *alpha-fetoprotein* (*Afp*), via section *in situ* hybridization (Fig. 2E, black dashed lines; n=4/4). When compared with the untreated controls, all of these BMS493 treated embryos appear to upregulate *Afp* in the dorsal liver bud (Fig. 2C, D).

To quantify the extent of specification within the putative hepatic domain, the ratio of HNF4α to PROX1 positive cells was compared between control and BMS493 treated embryos (Fig. 2F). In this manner, a modest but significant reduction in hepatic specification is observed in the dorsal anterior liver bud of BMS493 treated embryos compared to controls.

To determine the identity of the HNF4α-negative cells within the PROX1-positive dorsal liver bud, immunofluorescence was performed with other endoderm markers. Immunofluorescence of control embryos reveals the wild-type expression of ISL1 in the gut tube and sinus venosus [SV; Fig. 2C; (Mu et al., 2020)]. In contrast, a ventral expansion of the ISL1 positive cells into the dorsal liver bud is observed in BMS493 treated liver buds (Fig. 2C, white dashed line; n = 9/9) a condition not seen in the liver bud of controls (Fig. 2C, D; n = 0/8). The ectopic ISL1 expression in BMS493 treated embryos suggests that this population is unspecified foregut. The maintenance of the endoderm domain markers such as PROX1 and FOXA1, but absence of hepatic specification markers including HNF4a and *Afp* suggests that the foregut is primed to initiate hepatogenesis but that RA abrogation impairs hepatic specification.

Disrupted RA signaling in *Rdh10*$^{trex/trex}$ embryos leads to a similar anterior liver bud defect

To determine if the results observed *ex vivo* are recapitulated in RA signaling deficient embryos *in vivo,* we analyzed E9.5 *Rdh10*$^{trex/trex}$ embryos. RDH10 is the sole enzyme that catalyzes the first oxidation step in RA synthesis that is essential for embryonic development (Kumar et al., 2012; Sandell et al., 2012; Sandell et al., 2007). *Rdh10*$^{trex/trex}$ embryos are homozygous for a point mutation in *Rdh10* that leads to an almost complete loss of RA signaling activity throughout the embryo and lethality by E13.0 (Sandell et al., 2007). Compared with their somite stage matched control littermates at E9.5, no significant developmental delay is observed in the *Rdh10*$^{trex/trex}$ embryos, consistent with published results [Fig. 3A–B; (Sandell et al., 2007)]. Sectioned immunofluorescence of mutant liver buds reveals a similar, yet more severe, phenotype to that observed after BMS493 treatment (Fig. 3D). The anterior liver buds of *Rdh10*$^{trex/trex}$ embryos are noticeably smaller than controls, and although this smaller liver bud is uniformly PROX1 positive, it lacks HNF4α in the dorsal half. As observed with BMS493 treated embryos, the middle of *Rdh10*$^{trex/trex}$ liver buds are comparable to controls and are uniformly populated by PROX1 and HNF4α positive cells. At E9.5 an abnormal anterior liver bud is observed in 8/10 *Rdh10*$^{trex/trex}$ embryos and 0/9 control embryos (*Rdh10*$^{+/+}$ and *Rdh10*$^{trex/+}$). Quantification of the extent of hepatic specification in the presumptive hepatic domain reveals a significant decrease

in HNF4α-positive specified hepatoblasts in the dorsal anterior and ventral middle portion of *Rdh10*$^{trex/trex}$ embryos compared to littermate controls (Fig. 3E). These results confirm our *ex vivo* data and further highlight the importance of RA signals for appropriate hepatic specification *in vivo*.

Mesodermal disorganization adjacent to the developing liver bud in RA impaired embryos

The mesoderm surrounding much of the E9.5 liver bud includes the STM (Fig. 4A–L, lollipop). The exception includes the anterior-most liver bud, which is bounded anteriorly by the bilaterally symmetric SV (Fig. 4A–L, arrows) and the dorsal-most liver bud which contacts the coelomic mesothelial cavities (Fig. 4A–L, arrowheads). These features are perhaps more easily observed in transversely sectioned control embryos in which immunohistochemistry for HNF4α and eosin counterstaining was performed (Fig. 4A, B and I, J). We noted that the coelomic cavities were often missing or severely reduced in BMS493-treated or *Rdh10*$^{trex/trex}$ embryos, while the SV was thickened and disorganized (compare Fig. 4A, B to E, F and I, J to K, L). To further analyze the mesoderm surrounding the impaired liver bud of BMS493 treated embryos, immunofluorescence was performed with the mesoderm markers GATA4 and ISL1. GATA4 is normally expressed in the STM and in the SV while ISL1 is expressed in the SV and gut tube. In controls, the densely populated GATA4 positive STM uniformly surrounds the developing ventral liver bud (Fig. 4C–D, lollipop) while an organized ISL1 positive SV surrounds the dorsal liver bud (Fig. 4C–D, arrows). In BMS493 treated embryos, although GATA4 expression in the STM surrounding the ventral liver bud appears normal (Fig. 4G–H, lollipop), ISL1 and GATA4 expression surrounding the dorsal unspecified portion of the liver bud is reduced and this dorsal mesoderm lacks the organization observed in controls (Fig. 4G, H).

Characterization of the mid-gestation liver defect observed in RA signaling deficient embryos

To better understand how RA abrogation affects the liver, we next examined E10.0–10.5 *Rdh10*$^{trex/trex}$ and littermate controls. Between E10.0–11.0 the liver bud proliferates rapidly (Ogoke et al., 2022) and by ~E10.0, the liver is comprised of a large centrally located rostral lobe and two smaller and bilateral dorsal/caudal lobes. To view the rostral and caudal lobes in the same section, embryos were oriented with the anterior-posterior axis at a 45° angle in an “off-frontal” position for sectioning (Fig. 5A, B, dashed line indicates plane of section). In E10.5 controls, HNF4α positive hepatoblasts are distributed throughout the GATA4-positive hepatic mesoderm of both the rostral lobe (Fig. 5A’, blue asterisk) and the smaller caudal lobes (Fig. 5A’, yellow asterisks). In the E10.5 *Rdh10*$^{trex/trex}$ embryos, the characteristic tightly organized GATA4 positive dorsal lobe mesoderm is lost or severely reduced (Fig. 5B’). The dorsal lobe loss is also apparent after hematoxylin and eosin (H&E) staining of the same sections. The dorsal lobe defect is observed in 4/5 E10.0–10.5 *Rdh10*$^{trex/trex}$ embryos and 0/7 control embryos. In addition, two of the E10.5 *Rdh10*$^{trex/trex}$ embryos examined had an even more severe hepatic phenotype, containing few to no HNF4α positive hepatoblasts and a dramatic loss of identifiable hepatic mesenchyme (SFig. 2). Analysis of E12.5 whole mount *Rdh10* control and *Rdh10*$^{trex/trex}$ livers confirms the absence/reduction of the dorso-caudal lobes in *Rdh10*$^{trex/trex}$ embryos [Fig. 5C–D; (Sandell et al., 2007)]. *RARE-lacZ* staining of *Rdh10* control and *Rdh10*$^{trex/trex}$ whole mount E12.5

livers (Fig. 5E–F) reveals that RA signaling is highly active and specific to the dorsal mesoderm of *Rdh10* control livers, adjacent to the developing caudal lobes. This *RARE-lacZ* stained mesoderm is not observed in *Rdh10*$^{trex/trex}$ livers and notably the RA signaling activity in the dorsal mesoderm correlates to the disorganized mesoderm observed in E9.5 RA disrupted embryos (Fig. 4) as well as the lack of caudal lobe mesoderm at E10.5 (Fig. 5).

Exogenous RA also impairs early liver development

While RA inhibition has an adverse impact on liver development in zebrafish and medaka (Negishi et al., 2010; Stafford and Prince, 2002), excess RA results in a complete loss or reduction of liver markers in *Xenopus* and chick (Bayha et al., 2009; Chen et al., 2004). To determine the effect of excess RA on murine hepatic specification, we cultured pre-hepatic embryos (E8.25; 4–6S) through the liver budding stage (E9.5; 24–28S) with exogenous RA (Fig. 6A, B; 0.25–0.5 μM). The efficacy of exogenous RA administration was confirmed by the expanded expression of the RA target gene, *Hoxa1*, in RA treated embryos when compared to cultured controls [Fig. 6A, B; (Savory et al., 2014)].

Control and RA treated embryos were analyzed with liver and foregut specific markers (Fig. 6C, D). Overall, RA supplementation leads to a more severe hepatic phenotype than that observed with RA inhibition. Ectopic RA produces livers that fail to thicken or invade the surrounding mesoderm. In RA treated embryos, PROX1-positive cells are observed throughout the presumptive liver bud but HNF4α-expressing hepatoblasts are sparsely distributed (n = 8/9) compared to controls (n = 2/10). Furthermore, a small population of ISL1-positive cells is consistently observed in the RA treated liver bud (n = 8/9), which is only rarely observed in controls (n = 2/10). Consistent with the loss of HNF4α in the RA treated embryos, *Afp* is highly reduced throughout the liver bud (n = 3/3) when compared to controls (Fig. 6E). In contrast to that observed upon RA signaling loss presented above, the mesoderm surrounding the impaired liver bud in RA-treated embryos is organized and appears normal. To determine the extent of specification within the control and RA-treated liver buds, the ratio of HNF4α/PROX1 positive cells was calculated, revealing a significant reduction in hepatic specification throughout the liver bud of RA treated embryos compared to controls (Fig. 6F). Together these results demonstrate that high levels of RA profoundly inhibit normal hepatic development.

Discussion

RA signaling plays a critical role in posterior foregut endoderm development in a number of lower vertebrates. Herein we demonstrate that endogenous RA gradients are required for appropriate hepatic specification in mammals. We demonstrate that RA signal reduction via small molecule application in whole embryo culture leads to a slight but significant loss of specified hepatoblasts in the dorsal portion of the anterior liver bud and that this phenotype is more significantly recapitulated in *Rdh10*$^{trex/trex}$ mutants. In both the *in vitro* and *in vivo* models of RA abrogation, uniform expression of FOXA1 and PROX1is observed throughout the entire liver bud, while hepatoblast markers are significantly diminished in the dorsal/anterior portion of the PROX1 defined hepatic domain. Together these results demonstrate

that RA signals play a role in the appropriate specification of a subset of hepatoblasts and that it is not required for foregut patterning.

Given the critical role for RA in hepatic specification in lower vertebrates, this regional reduction in hepatic specification likely explains why a role for RA in early liver development has been overlooked in previous mammalian studies. In other mammalian studies examining the role of RA in organogenesis, hepatic domain markers rather than hepatic specification markers were examined and only a slight reduction was observed (Molotkov et al., 2005; Wang et al., 2006). For example, although the nascent liver was clearly abnormal *Aldh1a2* −/− embryos, because the resultant embryos expressed the hepatic markers *Prox1* and *Hex* in the ventral foregut the authors concluded that RA signaling was not required for liver induction (Martin et al., 2005; Molotkov et al., 2005).

Evidence provided herein and elsewhere suggests that RA signaling plays a direct role in specifying the hepatic endoderm, however as noted below it is also possible that RA's role in hepatic specification is indirectly supported by its activity in the adjacent inductive mesoderm. We have demonstrated that at least one RAR and one RXR are expressed in the liver progenitors at E8.5 and the liver bud at E9.5, providing evidence that the pre-hepatic and early liver bud endoderm are each capable of directly responding to RA signals. While expression of the RA synthesis enzyme *Aldh1a2* in the SV and other dorsal mesoderm suggests that RA is produced by the mesoderm, expression of the RA reporter construct *RARE-lacZ* demonstrates that RA is normally active in the dorsal endoderm (Molotkov et al., 2005; Rankin et al., 2018). RA signaling has specifically been found to be active in the posterior foregut at E8.25, at the point of liver induction, as well as E9.5, during liver bud development (Mic et al., 2002; Molotkov et al., 2005). Herein we demonstrate that RA signaling is active in the mesoderm adjacent to the hepatic progenitors at E8.5 and the dorsal hepatoblasts and adjacent dorsal mesenchyme in the nascent liver bud by E9.5. Furthermore, recent single cell RNA sequencing of FoxA2 positive cells found an upregulation of the LXR/RXR signaling pathway in the developing liver bud compared to the adjacent gut tube (Mu et al., 2020). RA signaling activity in the endoderm and upregulation of the RXR signaling specifically in the liver bud suggests RA signaling via RAR/RXR has a direct role during hepatic specification. It is important to note that we also describe defects in the mesoderm that supports the afflicted hepatic endoderm in both our *ex vivo* and *in vivo* models of RA abrogation and recent single cell analysis of early hepatic mesoderm/endoderm is supportive of a direct role for RA in the hepatic mesenchyme (Han et al., 2020). Therefore, we cannot rule out the fact that the supportive mesoderm may require RA directly and the affects observed in the hepatoblasts are secondary to this requirement.

Our results demonstrating a key role for Rdh10 and RA signaling in early hepatic progenitor cell differentiation are also supported by studies of E14.5 hepatic progenitor cells in which RA signaling components and coregulators have been detected. Moreover, exogenous RA induces markers of terminal hepatic differentiation and glycogen synthesis as an indicator of mature hepatocyte function (Huang et al., 2009). Thus, RA is required for both the initiation of hepatocyte progenitor cell differentiation and for terminal hepatocyte differentiation.

It should be noted that while both RA signal inhibition and ectopic RA each result in impaired hepatic specification, they are not similarly impaired. In RA deficient embryos, the dorsal/anterior liver bud is most prominently impaired while ectopic RA affects the entire liver bud. This result can be explained in part by the expression data presented herein. RA activity, revealed by *RARE-lacZ* expression, is confined to the mesenchyme dorsal to the hepatic progenitors during early hepatogenesis and to the nascent dorsal liver bud and its associated mesenchyme slightly later (Fig. 1F). An explanation for the dorsal hepatic loss is that RA is required for hepatic induction/specification in the portion of the organ closest to the RA signals. These expression patterns do not explain why this loss is confined to the dorsal/anterior but does not affect the dorsal/posterior. On the other hand, the expression of the RA receptors, *Rara, Rarb* and *Rxra,* indicate that the entire hepatic domain is poised to be activated by ectopic RA (Fig. 1 A–C) where, in accordance with the data presented herein, high levels of RA inhibit hepatic specification.

Others have noted the apparent lack of a relationship between alteration of the RA gradient and the resultant developmental phenotype in other tissues, such as limbs and heart, where excess RA and RA inhibition can each impair development (Bernheim and Meilhac, 2020). While it might seem paradoxical that hepatic malformations occur from both a deficiency and excess of RA, an analogous phenomenon has also been observed with respect to congenital anomalies in human patients exposed to retinoid or RAR-agonist based drugs, and from vitamin A-deficiency (Shannon et al., 2017). Each of these examples highlight the importance of strict control of the endogenous RA gradient during development.

Methods

In situ hybridization

In situ hybridization probes were made using the primers listed below (given 5’ to 3’). *Rarα* (forward) CCCTACGCCTTCTTCTTTCCC and (reverse) GTTTCGCACCGACTCCTTGG. *Rarβ* (forward) CTCCACTTCCTCCTCCTCGG and (reverse) AGGCGGCTTTGAGCAGGG. *Rxrα* (forward) CCTACACCTGCCGAGACAAC and (reverse) GAGAATCCCATCTTTCACAGC. *Rdh10* (forward) GAAATCCTGCCCCCGTGT and (reverse) CCGTGTCTACAAGGTAAGGGC. *Aldh1a2* (forward) TCTGTTGGACAAGCTTGCAG and (reverse) CAGCGTAGTCCAAGTCAGC.A *Pax9* (forward) ACGACTCATACAAGCAGCACCA and (reverse) CACATAACCAGAAGGAGCAGCA. *Hoxa1* (forward) CCTTATGGCCCCTATGGATT and (reverse) CCTGGGTCTCATTGAGCTGT. RT-PCR was performed using E9.5 cDNA and amplified PCR products were cloned into a pCR™4-TOPO® TA vector using the TOPO® TA Cloning® Kits for Sequencing (Invitrogen). Plasmids were linearized and *in vitro* transcription was performed using T3/T7 RNA polymerase (Roche) and DIG RNA labeling mix (Roche) to generate the anti-sense DIG-labeled RNA probes. The *Afp* probe was described (Wang et al., 2015*)*. Embryos for *in situ* hybridization were collected from CD-1 mice (Charles River, bred in house), fixed in 4% PFA overnight at 4 °C, rinsed in DEPC-treated PBT, and dehydrated in methanol. Whole mount *in situ* hybridization was performed as described (Archambault et al., 2020) and section *in situ* hybridization performed as described (Wang et al., 2015*)*. Slides were cover slipped with Cytoseal 60 and imaged

using a Panoramic MIDI slide scanner (3DHistech) or a Nikon Eclipse Ti2-S-U inverted microscope with a DS-Ri2 camera and NIS Elements imaging software. Whole-mount images were taken after dehydration on a Nikon SMZ1500 dissecting microscope with a SPOT model 29.2–1.3 MP color camera and SPOT 5.6 software.

Whole embryo culture and small molecule RA signaling inhibition

Animal studies are approved by the University of Massachusetts, Amherst's Institutional Animal Care and Use Committee (IACUC protocol# 2018–0045). CD-1 mice (Charles River, bred in house) were used for mating and the morning a vaginal plug was observed was defined as E0.5. Embryos were collected at E8.25 and the decidua and Reichert's membrane were removed in low O_2-equilibriated dissection media on a 37 °C hot plate, leaving the yolk sac and ectoplacental cone intact. Dissection and culture media were prepared as previously described (Angelo et al., 2012). Embryos were maintained at 37 °C in a low O_2 (5%) incubator until all embryos were collected (<1 hr). For long term culture, embryos were placed in glass bottles with at least 0.5 mL of 25% culture media and 75% heat inactivated rat serum per embryo (a minimum of 1.5 mL media/ bottle). For RA signaling inhibition, 20 μM of the small molecule pan-RAR inverse agonist BMS493 (Tocris) was added to the media, the highest concentration that still yielded grossly normal embryos. Exogenous RA (Sigma) was added to media at a concentration of 0.25 μM or 0.5 μM. Dimethyl sulfoxide (DMSO) was used as a diluent for both drugs and an equal volume of DMSO was added to the culture media of control embryos during each experiment. All embryos were initially gassed with 5% oxygen and incubated at 37 °C on a roller incubator for ~36 hours total and were subsequently gassed with 20% oxygen every 12 hours. Whole-mount images of cultured embryos were taken after dehydration on a Nikon SMZ1500 dissecting microscope with a SPOT model 29.2–1.3 MP color camera and SPOT 5.6 software.

Rdh10$^{trex/trex}$ and *RARE-lacZ* mice

Rdh10$^{trex/+}$ mice were maintained and genotyped as previously described (Sandell et al., 2007), and *Rdh10*$^{trex/+}$ mice were intercrossed to generate *Rdh10*$^{trex/trex}$ embryos. The *RARE–lacZ* transgenic mice were maintained as previously described (Rossant et al., 1991) and males were interbred with female *Rdh10*$^{trex/+}$ mice. Male *Rdh10*$^{trex/+}$*; RARE–lacZ* mice were then intercrossed with female *Rdh10*$^{trex/+}$ mice to generate *Rdh10*$^{trex/trex}$*; RARE-lacZ* embryos.

All experiments on these animals were performed in accordance with the guidelines of the Stowers Institute for Medical Research Animal Care and Use Committee approved protocol (IACUC #2019–097).

Whole mount imaging and LacZ staining of *RARE-lacZ* tissues

Embryos were isolated from the uteri, and dissected livers or whole embryos fixed in 4% paraformaldehyde overnight at 4 °C for bright field microscopy, or fixed in 0.2% glutaraldehyde/2% formalin in PBS for 1h in an ice-water bath for lacZ staining. For lacZ staining, fixed livers were then washed for 3 × 15 minutes in cold PBS, rinsed in warmed (37 °C) staining buffer (5mM potassium ferricyanide, 5mM potassium ferrocyanide, 2mM

MgCl, 0.01%sodiumdeoxycholate, 0.02% NonidetP-40) for 5–10 minutes, before being incubated in X-gal (40mg/ml) in staining buffer overnight at 37 °C and photographed with bright field microscopy. Whole lacZ stained embryos were dehydrated in ethanol, cleared in xylene, embedded in paraffin wax, and serially sectioned (7 μm). Slides were cover slipped with Cytoseal 60 and imaged on a Nikon Eclipse Ti2-S-U inverted microscope with a DS-Ri2 camera and NIS Elements imaging software.

Histology and Immunofluorescence

Embryos were fixed in 4% PFA overnight at 4 °C, rinsed in PBS, dehydrated in ethanol, cleared in xylene, embedded in paraffin wax, and serially sectioned (7 μm). E9.5 embryos were positioned in a transverse or sagittal orientation for analysis. E10.0 and E10.5 embryos were oriented with the anterior-posterior axis at a 45° angle in an off-frontal position instead of the 90° angle in a transverse orientation. For immunofluorescence, deparaffinized and rehydrated slides were subjected to antigen retrieval via boiling in Tris-EDTA buffer (pH 9) and then allowed to cool to room temperature. Blocking occurred at room temperature for 2 hours in 0.5% dry milk in PBT before primary antibody incubation (diluted in 0.005% milk block) overnight at 4 °C. The primary antibodies and working dilutions used are as follows; goat anti-HNF4α (Santa Cruz, sc6556, 1:200), rabbit anti-Prox1 (Angiobio, 11–002P, 1:200), mouse anti-ISL1 (Hybridoma Bank, 40.2D6, 1:200), rabbit anti-GATA4 (SantaCruz, sc9053, 1:250). Slides were incubated with secondary antibodies (diluted in 0.005% milk block) for 1 hour at room temperature. The secondary antibodies and dilutions used are as follows; Alexa Fluor 488, 546, and 647 donkey antibodies (Molecular Probes, 1:500). Slides were counterstained with DAPI (Roche) and cover slipped with ProLong™ Gold antifade reagent (Invitrogen). Slides were then imaged on a Nikon Eclipse Ti inverted microscope with an Andor DR-228C camera and NIS Elements imaging software or on a Panoramic MIDI slide scanner (3DHistech).

Immunohistochemistry

For immunohistochemistry, deparaffinized and rehydrated slides were subjected to antigen retrieval via boiling in Tris-EDTA buffer (pH 9) and then allowed to cool to room temperature. Endogenous peroxidases were removed by treating slides with 0.3 % H_2O_2. Blocking occurred at room temperature for 2 hours in 0.5% dry milk in PBT before primary antibody incubation (diluted in 0.005% milk block) overnight at 4 °C. The primary antibody and working dilution used are as follows; goat anti-HNF4α (Santa Cruz, sc6556, 1:200). Slides were incubated with secondary antibodies (diluted in 0.005% milk block) for 1 hour at room temperature. The secondary antibody and dilution used are as follows; biotinylated rabbit anti-goat IgG (H+L) (Vector Labratories, BA-5000, 1:1000). Slides were incubated with an avidin-biotin complex (ABC Peroxidase Staining Kit, ThermoFisher 32020) for 30 minutes at room temperature. Detection was performed using 1x DAB substrate solution (Metal Enhanced DAB Substrate Kit, ThermoFisher, 34065) and allowed to proceed until color development was sufficient. Slides were counterstained with Eosin Y (Polysciences, Inc.), cover slipped with Cytoseal 60, and then imaged on a Panoramic MIDI slide scanner (3DHistech).

Hematoxylin and Eosin (H&E) Staining

H&E staining was performed post-immunofluorescence after coverslips were removed by soaking slides in PBS. Slides were submerged in distilled water before being stained with Hematoxylin+ (Fisher HealthCare™) for 30 seconds. Slides were rinsed under gentle running tap water for 1 minute, treated with 0.3% acid alcohol for 30 seconds, and then submerged in tap water followed by Modified Scott's Tap Water Substitute (Hito) for 1 minute each. Slides were rinsed in tap water and dipped in 90% ethanol before being stained with Eosin Y (Polysciences, Inc.) for 30 seconds. Slides were rinsed twice in 90% ethanol followed by 100% ethanol for 1 minute each before a 2-minute xylene wash. Slides were then cover slipped with Cytoseal 60 and imaged with a Nikon Eclipse Ti2-S-U inverted microscope with a Photometrics Iris 15™ sCMOS camera and NIS Elements imaging software.

Data Analysis

All cell counting data was performed with transverse sections of somite matched E9.5 cultured control and BMS493-treated embryos. IF was performed with HNF4α and PROX1 and counterstained with DAPI. All sections containing the liver bud were counted and then divided equally into anterior, middle, and posterior thirds. The dorsal and ventral portion of the liver bud on each section was determined by dividing the area of the PROX1 expressing hepatic domain in half. All HNF4α and PROX1 positive cells were counted in the dorsal and ventral halves of alternating sections of each liver bud. The ratio of HNF4α/PROX1 positive cells in each section was calculated to indicate the extent of specified hepatoblasts and to normalize for an overall size reduction of the hepatic domain. For statistical analysis, a Student's *t* test assuming unequal variance was performed between the average ratio of HNF4α/PROX1 positive cells of control and BMS493 treated embryos. The same process was repeated with *Rdh10* control and $Rdh10^{trex/trex}$ as well as control and RA treated stage matched E9.5 embryos.

Supplementary Material

Refer to Web version on PubMed Central for supplementary material.

Acknowledgements

We thank members of the Tremblay and Mager labs for their input and advice. Some of the original data underlying this manuscript can be accessed from the Stowers Original Data Repository at http://www.stowers.org/research/publications/libpb-xxxx".

Funding

This work was supported by Stowers Institute for Medical Research (1008) to PAT and by the National Institute of Health (R01 DK123363) to KDT.

References

Abu-Abed S, Dolle P, Metzger D, Wood C, MacLean G, Chambon P, Petkovich M, 2003. Developing with lethal RA levels: genetic ablation of Rarg can restore the viability of mice lacking Cyp26a1. Development 130, 1449–1459. [PubMed: 12588859]

Angelo JR, Guerrero-Zayas MI, Tremblay KD, 2012. A fate map of the murine pancreas buds reveals a multipotent ventral foregut organ progenitor. PLoS ONE 7, e40707. [PubMed: 22815796]

Archambault D, Cheong A, Iverson E, Tremblay KD, Mager J, 2020. Protein phosphatase 1 regulatory subunit 35 is required for ciliogenesis, notochord morphogenesis, and cell-cycle progression during murine development. Dev Biol 465, 1–10. [PubMed: 32628936]

Bayha E, Jorgensen MC, Serup P, Grapin-Botton A, 2009. Retinoic acid signaling organizes endodermal organ specification along the entire antero-posterior axis. PLoS ONE 4, e5845. [PubMed: 19516907]

Bernheim S, Meilhac SM, 2020. Mesoderm patterning by a dynamic gradient of retinoic acid signalling. Philos Trans R Soc Lond B Biol Sci 375, 20190556. [PubMed: 32829679]

Chazaud C, Chambon P, Dolle P, 1999. Retinoic acid is required in the mouse embryo for left-right asymmetry determination and heart morphogenesis. Development 126, 2589–2596. [PubMed: 10331971]

Chen Y, Pan FC, Brandes N, Afelik S, Solter M, Pieler T, 2004. Retinoic acid signaling is essential for pancreas development and promotes endocrine at the expense of exocrine cell differentiation in Xenopus. Dev Biol 271, 144–160. [PubMed: 15196957]

Desai TJ, Malpel S, Flentke GR, Smith SM, Cardoso WV, 2004. Retinoic acid selectively regulates Fgf10 expression and maintains cell identity in the prospective lung field of the developing foregut. Dev Biol 273, 402–415. [PubMed: 15328022]

Farjo KM, Moiseyev G, Nikolaeva O, Sandell LL, Trainor PA, Ma JX, 2011. RDH10 is the primary enzyme responsible for the first step of embryonic Vitamin A metabolism and retinoic acid synthesis. Dev Biol 357, 347–355. [PubMed: 21782811]

Han L, Chaturvedi P, Kishimoto K, Koike H, Nasr T, Iwasawa K, Giesbrecht K, Witcher PC, Eicher A, Haines L, Lee Y, Shannon JM, Morimoto M, Wells JM, Takebe T, Zorn AM, 2020. Single cell transcriptomics identifies a signaling network coordinating endoderm and mesoderm diversification during foregut organogenesis. Nat Commun 11, 4158. [PubMed: 32855417]

Huang J, Bi Y, Zhu GH, He Y, Su Y, He BC, Wang Y, Kang Q, Chen L, Zuo GW, Luo Q, Shi Q, Zhang BQ, Huang A, Zhou L, Feng T, Luu HH, Haydon RC, He TC, Tang N, 2009. Retinoic acid signalling induces the differentiation of mouse fetal liver-derived hepatic progenitor cells. Liver Int 29, 1569–1581. [PubMed: 19737349]

Kumar S, Sandell LL, Trainor PA, Koentgen F, Duester G, 2012. Alcohol and aldehyde dehydrogenases: retinoid metabolic effects in mouse knockout models. Biochimica et biophysica acta 1821, 198–205. [PubMed: 21515404]

Martin M, Gallego-Llamas J, Ribes V, Kedinger M, Niederreither K, Chambon P, Dolle P, Gradwohl G, 2005. Dorsal pancreas agenesis in retinoic acid-deficient Raldh2 mutant mice. Dev Biol 284, 399–411. [PubMed: 16026781]

Mic FA, Haselbeck RJ, Cuenca AE, Duester G, 2002. Novel retinoic acid generating activities in the neural tube and heart identified by conditional rescue of Raldh2 null mutant mice. Development 129, 2271–2282. [PubMed: 11959834]

Molotkov A, Molotkova N, Duester G, 2005. Retinoic acid generated by Raldh2 in mesoderm is required for mouse dorsal endodermal pancreas development. Dev Dyn 232, 950–957. [PubMed: 15739227]

Mu T, Xu L, Zhong Y, Liu X, Zhao Z, Huang C, Lan X, Lufei C, Zhou Y, Su Y, Xu L, Jiang M, Zhou H, Lin X, Wu L, Peng S, Liu S, Brix S, Dean M, Dunn NR, Zaret KS, Fu XY, Hou Y, 2020. Embryonic liver developmental trajectory revealed by single-cell RNA sequencing in the Foxa2(eGFP) mouse. Commun Biol 3, 642. [PubMed: 33144666]

Negishi T, Nagai Y, Asaoka Y, Ohno M, Namae M, Mitani H, Sasaki T, Shimizu N, Terai S, Sakaida I, Kondoh H, Katada T, Furutani-Seiki M, Nishina H, 2010. Retinoic acid signaling positively regulates liver specification by inducing wnt2bb gene expression in medaka. Hepatology (Baltimore, MD) 51, 1037–1045.

Niederreither K, McCaffery P, Drager UC, Chambon P, Dolle P, 1997. Restricted expression and retinoic acid-induced downregulation of the retinaldehyde dehydrogenase type 2 (RALDH-2) gene during mouse development. Mech Dev 62, 67–78. [PubMed: 9106168]

Ogoke O, Guiggey D, Mon T, Shamul C, Ross S, Rao S, Parashurama N, 2022. Spatiotemporal imaging and analysis of mouse and human liver bud morphogenesis. Dev Dyn 251, 662–686. [PubMed: 34665487]

Palaria A, Angelo JR, Guertin TM, Mager J, Tremblay KD, 2018. Patterning of the hepato-pancreatobiliary boundary by BMP reveals heterogeneity within the murine liver bud. Hepatology (Baltimore, MD) 68, 274–288.

Rankin SA, McCracken KW, Luedeke DM, Han L, Wells JM, Shannon JM, Zorn AM, 2018. Timing is everything: Reiterative Wnt, BMP and RA signaling regulate developmental competence during endoderm organogenesis. Dev Biol 434, 121–132. [PubMed: 29217200]

Rossant J, Zirngibl R, Cado D, Shago M, Giguere V, 1991. Expression of a retinoic acid response element-hsplacZ transgene defines specific domains of transcriptional activity during mouse embryogenesis. Genes Dev 5, 1333–1344. [PubMed: 1907940]

Sandell LL, Lynn ML, Inman KE, McDowell W, Trainor PA, 2012. RDH10 oxidation of Vitamin A is a critical control step in synthesis of retinoic acid during mouse embryogenesis. PLoS ONE 7, e30698. [PubMed: 22319578]

Sandell LL, Sanderson BW, Moiseyev G, Johnson T, Mushegian A, Young K, Rey JP, Ma JX, Staehling-Hampton K, Trainor PA, 2007. RDH10 is essential for synthesis of embryonic retinoic acid and is required for limb, craniofacial, and organ development. Genes Dev 21, 1113–1124. [PubMed: 17473173]

Savory JG, Edey C, Hess B, Mears AJ, Lohnes D, 2014. Identification of novel retinoic acid target genes. Dev Biol 395, 199–208. [PubMed: 25251699]

Shannon SR, Moise AR, Trainor PA, 2017. New insights and changing paradigms in the regulation of vitamin A metabolism in development. Wiley Interdiscip Rev Dev Biol 6.

Stafford D, Prince VE, 2002. Retinoic acid signaling is required for a critical early step in zebrafish pancreatic development. Curr Biol 12, 1215–1220. [PubMed: 12176331]

Sucov HM, Dyson E, Gumeringer CL, Price J, Chien KR, Evans RM, 1994. RXR alpha mutant mice establish a genetic basis for vitamin A signaling in heart morphogenesis. Genes Dev 8, 1007–1018. [PubMed: 7926783]

Tremblay KD, Zaret KS, 2005. Distinct populations of endoderm cells converge to generate the embryonic liver bud and ventral foregut tissues. Dev Biol 280, 87–99. [PubMed: 15766750]

Wang J, Rhee S, Palaria A, Tremblay KD, 2015. FGF signaling is required for anterior but not posterior specification of the murine liver bud. Dev Dyn 244, 431–443. [PubMed: 25302779]

Wang Z, Dolle P, Cardoso WV, Niederreither K, 2006. Retinoic acid regulates morphogenesis and patterning of posterior foregut derivatives. Dev Biol 297, 433–445. [PubMed: 16806149]

Wendling O, Dennefeld C, Chambon P, Mark M, 2000. Retinoid signaling is essential for patterning the endoderm of the third and fourth pharyngeal arches. Development 127, 1553–1562. [PubMed: 10725232]

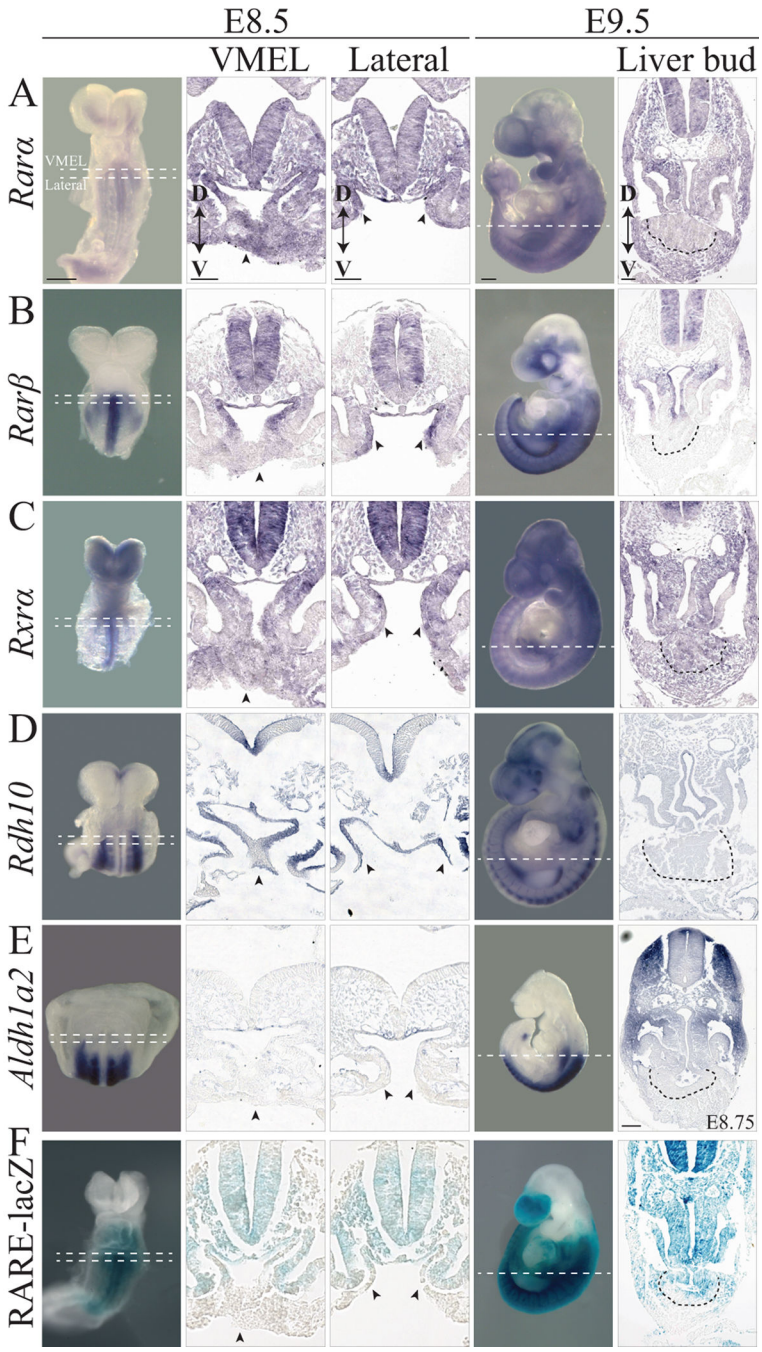

Fig. 1. Expression of RA signaling pathway components and RA signaling activity during hepatic specification.

In situ hybridization performed with the indicated probes (purple) or stained for β-galactosidase activity to reveal *RARE-lacZ* reporter expression (blue) in the VMEL and lateral liver progenitors (arrowheads) at E8.5 and liver bud (black dashed lines) at E9.5. The sections in A-C utilized the same probe as in the whole mount but *in situ* was performed directly on the sections. The sections in D-E were produced by sectioning the depicted whole mount depicted. The white dashed lines in the whole mount image depict the approximate plane of the sections to the right. The dorsal to ventral axis is indicated.

A) *Rarα* is expressed in the hepatic progenitors and surrounding mesoderm at E8.5 and at E9.5 in the liver bud and surrounding mesoderm. B) *Rarβ* is elevated in the dorsal endoderm and liver progenitors compared with the surrounding mesoderm at E8.5. By E9.5 *Rarβ* is absent from the liver bud and surrounding mesoderm. C) *Rxrα* is expressed uniformly in the pre-hepatic and hepatic domains and adjacent mesoderm at both E8.5 and E9.5. D) *Rdh10* is expressed in both liver progenitors and in adjacent tissues at E8.5 however not as highly in the liver bud or adjacent mesoderm at E9.5. E) *Aldh1a2* is not expressed in either the pre-hepatic or hepatic endoderm, however it is expressed in the dorsal endoderm at E8.5 and in a clear dorsal to ventral gradient at E8.75. F) The *RARE-lacZ* reporter is expressed in the mesoderm adjacent to the pre-hepatic endoderm, but not in the pre-hepatic endoderm at E8.5 and in the mesoderm adjacent to the dorsal liver bud and in the dorsal liver bud itself at E9.5. Scale bars on whole mount images: 0.25 mm. Scale bars on sectioned images: 50 μm.

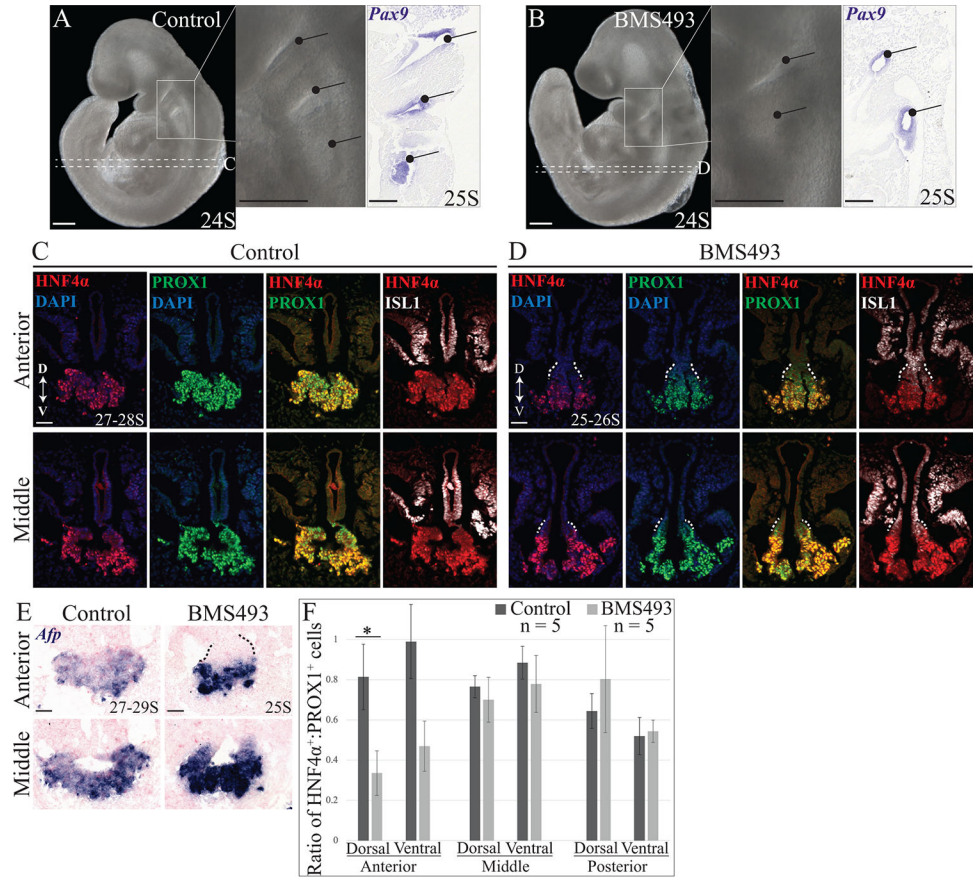

Fig. 2. RA signaling inhibition results in reduced dorsal/anterior hepatic specification.

A-B) Control and BMS493 treated embryos at the end of culture. Magnified pharyngeal region (white box) reveals the expected absence of the third pharyngeal pouch (lollipops) in BMS493 treated embryos (n = 44/47) compared to controls (n = 1/63). This loss was confirmed using *in situ* hybridization with a *Pax9* probe (n = 3). The white dashed lines indicate the approximate level of the sections in C-D. C-D) Immunofluorescence performed on transverse sections of control (left) and BMS493 treated (right) embryos with the hepatoblast specification marker HNF4α (red), the hepato-pancreatobiliary domain marker PROX1 (green), and the unspecified endoderm and sinus venosus (SV) marker, ISL1 (white). DAPI (blue) was used to visualize all nuclei. The dorso-ventral axis is indicated. HNF4α and PROX1 positive cells uniformly populate the entire control liver bud. While PROX1 positive cells uniformly populate the presumptive hepatic domain in BMS493 treated embryos, there is a noticeable reduction in HNF4α positive cells in the dorsal portion of the liver bud (white dashed lines). In the BMS493 treated embryos, ISL1 expands ventrally into the PROX1 portion of the liver bud (white dashed lines). E) *In situ hybridization* of transverse liver sections using the hepatic marker *Afp* (blue) and counterstained with eosin (pink), reveals a similar dorsal/anterior reduction of hepatoblasts in BMS493 treated embryos (black dashed lines, n = 4/4) compared to controls (n = 0/4). All 4 of the BMS493 treated embryos display a consistent upregulation of *Afp* in the hepatoblasts that remain compared with controls. F) Quantification of the ratio of HNF4α positive cells to PROX1 positive cells demonstrates the significant reduction of HNF4α

positive cells within the dorsal-anterior liver bud in the BMS493 treated embryos (n = 5) compared to controls (n = 5). *p= 0.0453. The somite stage (S) of each distinct embryo presented is indicated. Scale bars on whole mount images: 0.25 mm. Scale bars on sectioned images: 50 μm.

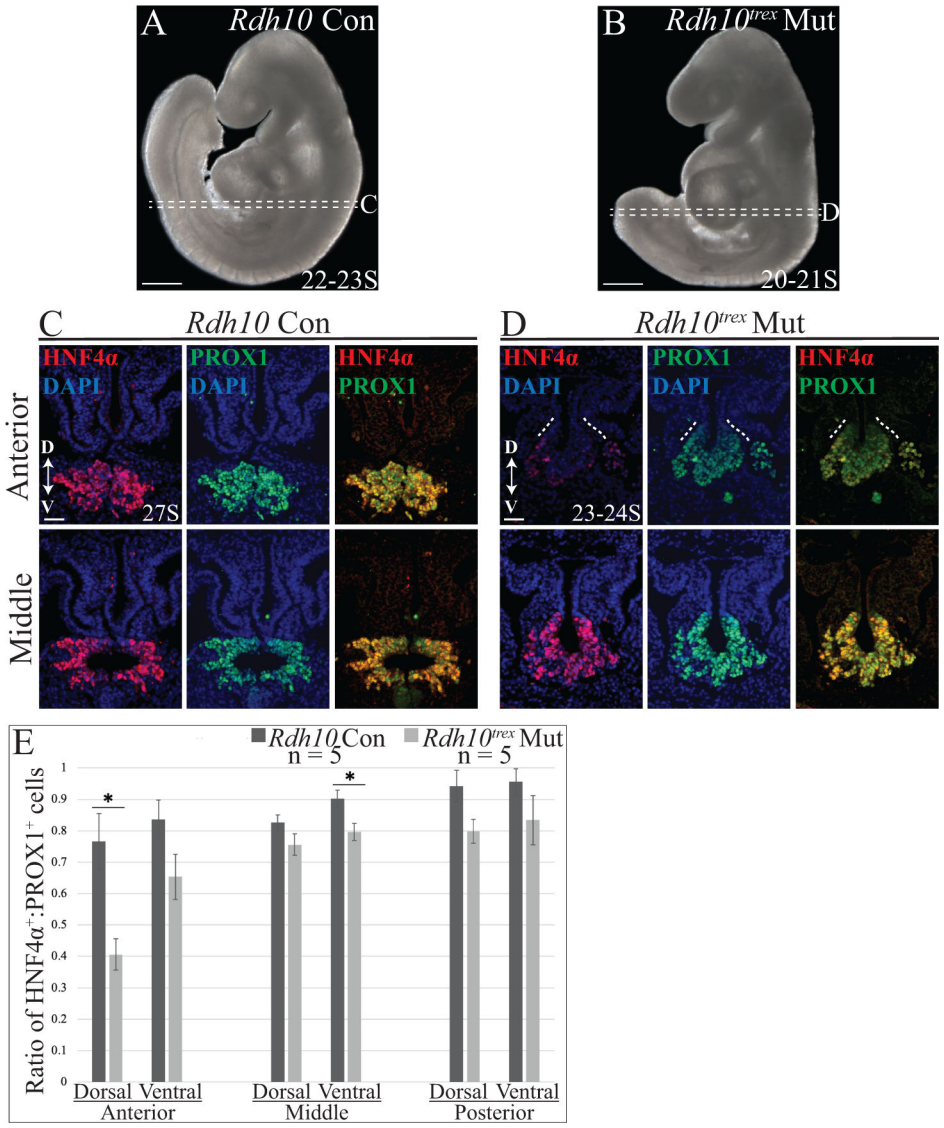

Fig. 3. Impaired hepatic specification in E9.5 *Rdh10*$^{trex/trex}$ embryos.

A-B) *Rdh10* control (*Rdh10*$^{+/+}$ / *Rdh10*$^{trex/+}$) and *Rdh10*^{trex} mutant (*Rdh10*$^{trex/trex}$) embryos. White dashed lines indicate the anterior and middle transverse sections taken through the liver bud shown in C-D. C-D) Immunofluorescence performed on *Rdh10* control (left) and *Rdh10*$^{trex/trex}$ (right) embryos with the hepatoblast marker HNF4α (red) and the hepato-pancreatobiliary domain marker PROX1 (green). DAPI (blue) was used to visualize all nuclei. The dorso-ventral axis is indicated. PROX1 positive cells uniformly populate the entire liver bud of *Rdh10* control and *Rdh10*$^{trex/trex}$ embryos. In *Rdh10*$^{trex/trex}$ embryos, a reduction in HNF4α positive cells is observed in the dorsal half of the anterior liver bud (indicated by white dashed lines) compared to the middle portion and the entire liver bud of *Rdh10* control embryos. E) Quantification of the ratio of HNF4α positive cells to PROX1 positive cells demonstrates that the significant reduction of HNF4α positive cells within the hepatic domain is limited to the dorsal portion of the anterior liver bud and ventral portion of the middle liver bud in *Rdh10*$^{trex/trex}$ embryos (n = 5) compared to controls (n = 5). *p= 0.01

for anterior dorsal and 0.03 for ventral middle. The somite stage (S) of each distinct embryo presented is indicated. Scale bars on whole mount images: 0.25 mm. Scale bars on sectioned images: 50 μm.

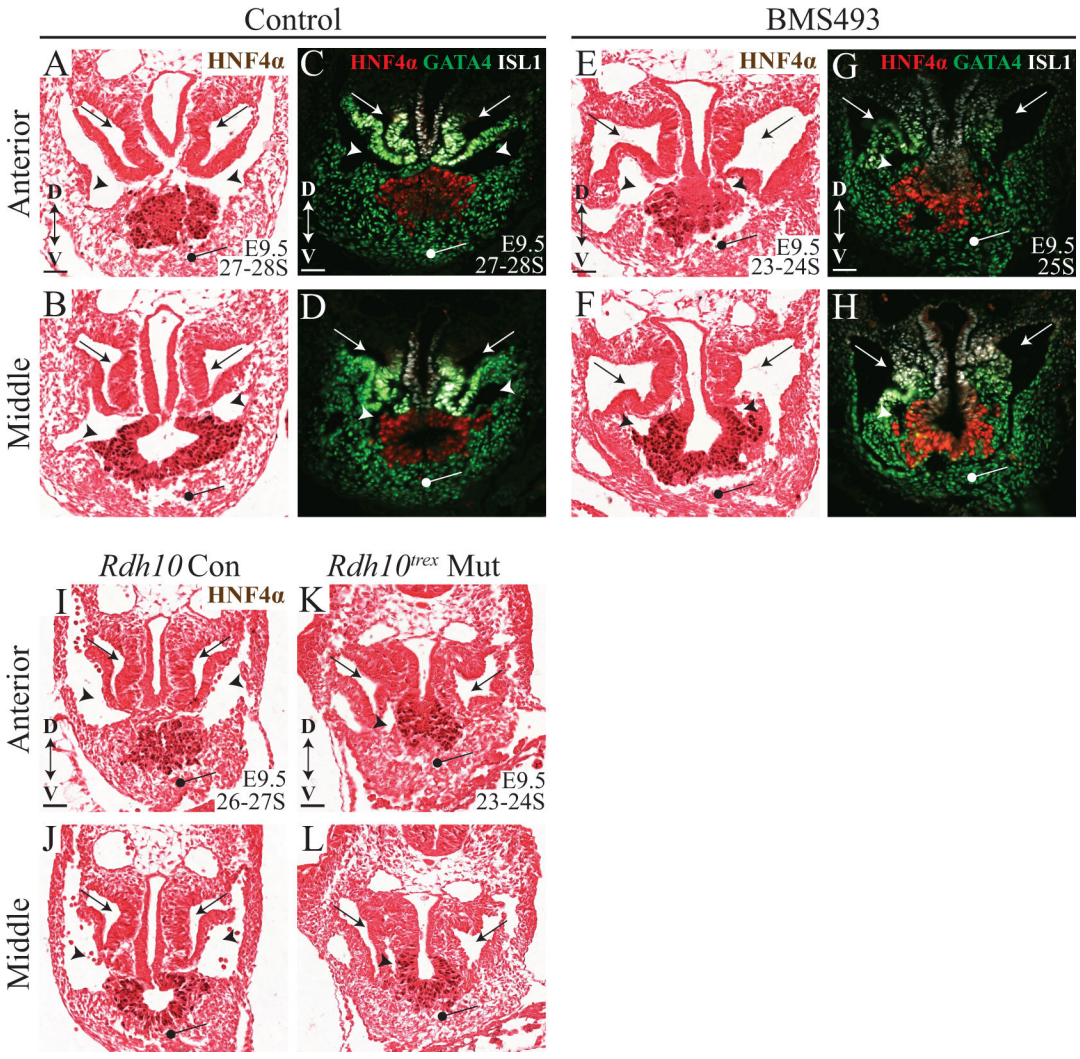

Fig. 4. Disorganized mesoderm in RA abrogated embryos.

A-H) Anterior and middle transverse sections through control and BMS493 treated E9.5 liver buds. The dorso-ventral axis is indicated. A-B, E-F) Immunohistochemistry with HNF4α (brown) and eosin counterstaining (pink) performed on E9.5 control and BMS493 treated sections. C-D, G-H) Immunofluorescence performed with HNF4α (red) and the mesoderm markers GATA4 (green) and ISL1 (white) on E9.5 control and BMS493 treated sections. A-D) Control liver buds are surrounded dorsally by an organized ISL1/GATA4 positive SV (arrows) and well defined coelomic mesothelial cavities (arrowheads), and ventrally by the GATA4 positive septum transversum mesenchyme (STM, lollipop). E-H) Unlike control embryos, BMS493 treated embryos often display aberrant ISL1 expression in the presumptive SV (arrows). The SV is disorganized and/or enlarged while the coelomic cavities (arrowheads) are reduced and abnormally positioned compared to controls. I-L) Immunohistochemistry with HNF4α (brown) and eosin counterstaining (pink) performed on E9.5 *Rdh10* control and *Rdh10*$^{trex/trex}$ transverse sections. Similar to the mesodermal defects observed in BMS493 treated embryos, while an STM (lollipop) surrounds the ventral liver bud, the dorsal mesoderm adjacent to the unspecified portion of the liver bud is largely

disorganized and abnormally positioned in the *Rdh10*$^{trex/trex}$ embryo. Structures resembling the SV are present (arrows) however the coelomic cavities (arrowheads) are either absent or much smaller than those observed in *Rdh10* controls.

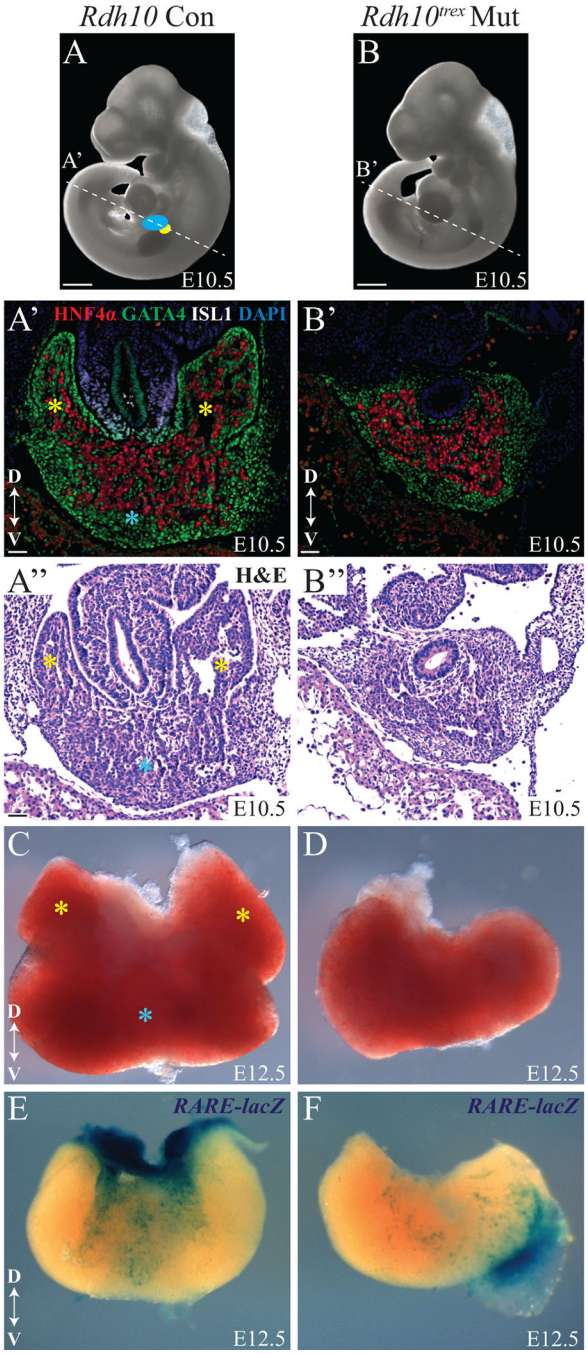

Fig. 5. Loss of the dorso-caudal lobes in E10.5 *Rdh10*$^{trex/trex}$ embryos.

A-B) E10.5 control (*Rdh10*$^{+/+}$ / *Rdh10*$^{trex/+}$) and *Rdh10*$^{trex/trex}$ mutant embryos. White dashed lines indicate the section taken through the liver shown in A'-B'. The rostral (blue asterisk) and caudal (yellow asterisks) lobes are shown in the whole mount control embryo. A'-B') Immunofluorescence performed on the embryos shown in A-B with the hepatoblast marker HNF4α (red) and mesoderm markers GATA4 (green) and ISL1 (white). DAPI (blue) was used to visualize all nuclei. In E10.5 *Rdh10* control embryos, HNF4α positive hepatoblasts populate the caudal lobes bounded by a tight GATA4 positive epithelial-like

cell lining (yellow asterisk) and are adjacent to the ISL1 positive coelomic mesothelium. Hepatoblasts also populate the rostral lobe bounded by the loosely organized GATA4 positive STM (blue asterisk). In contrast, *Rdh10*$^{trex/trex}$ embryos appear to consist mainly of a rostral lobe bounded by loosely organized GATA4 positive STM, while the caudal lobes are grossly reduced or absent. A”-B”) H&E staining performed on the sections shown in A’-B’. C-D) E12.5 whole mount *Rdh10* control and *Rdh10*$^{trex/trex}$ livers. While Rdh10 control livers consist of a rostral (blue asterisk) and two caudal lobes (yellow asterisks), Rdh10$^{trex/trex}$ livers appear to consist of only a rostral lobe. E-F) *RARE-lacZ* staining of E12.5 *Rdh10* control and *Rdh10*$^{trex/trex}$ whole mount livers show RA signaling activity highly specific to the dorsal mesoderm of *Rdh10* control livers which is absent from *Rdh10*$^{trex/trex}$ livers. The embryonic day of each distinct embryo presented is indicated. Scale bars on whole mount images: 0.25 mm. Scale bars on sectioned images: 50 μm.

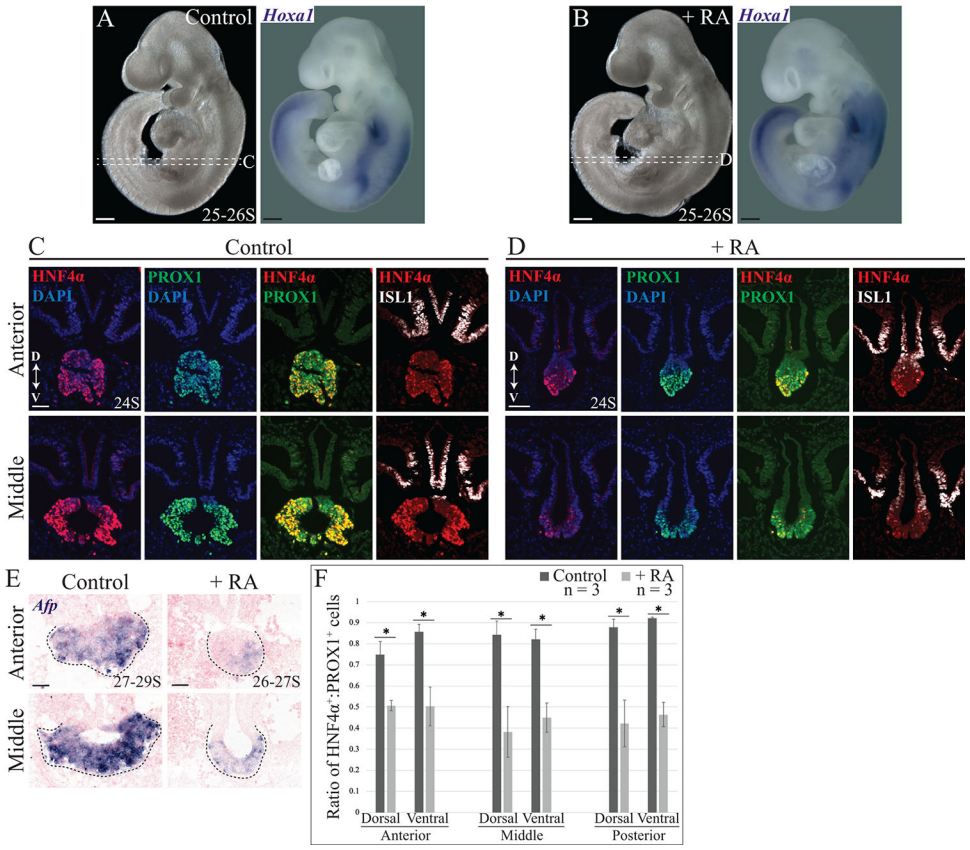

Fig. 6. Exogenous RA treatments leads to a severe early liver bud defect.

A-B) Control and RA treated embryos at the end of culture. *In situ* hybridization targeting the RA responsive gene *Hoxa1* (blue) demonstrates an upregulation and expansion of *Hoxa1* expression in RA treated embryos compared to controls, confirming effective exogenous RA treatment. White dashed lines indicate the anterior and middle transverse sections taken through the liver bud shown in C-D. C-D) Immunofluorescence performed on control (left) and RA treated embryos (right) with the hepatoblast marker HNF4α (red), hepato-pancreatobiliary domain marker PROX1 (green), and ISL1 (white). DAPI (blue) was used to visualize all nuclei. The dorso-ventral axis is indicated. Compared to controls, a much smaller liver bud is observed in the RA treated embryo. PROX1 positive cells uniformly populate the control and RA treated liver bud whereas HNF4α positive cells sparsely populate the RA treated liver bud. ISL1 positive cells are ectopically observed in the RA treated liver bud. E) *In situ* hybridization targeting the hepatic marker *Afp* (blue) performed on transverse sections of control and RA treated embryos confirms the abnormal liver bud (outlined in black dashed lines) observed in D. F) Quantification of the ratio of HNF4α positive to PROX1 positive cells reveals a statistically significant reduction in the number of specified hepatoblasts throughout the entire hepatic domain of RA treated embryos (n=3) compared to controls (n=3). *p= 0.045, 0.047, 0.042, 0.015, 0.043, 0.015; left to right. The somite stage (S) of each distinct embryo presented is indicated. Scale bars on whole mount images: 0.25 mm. Scale bars on sectioned images: 50 μm.